

# Electron and Hole $g$ Tensors of Neutral and Charged Excitons in Single Quantum Dots by High-Resolution Photocurrent Spectroscopy

Shiyao Wu,<sup>1,2</sup> Kai Peng,<sup>1,2</sup> Xin Xie,<sup>1,2</sup> Jingnan Yang,<sup>1,2</sup> Shan Xiao,<sup>1,2</sup> Feilong Song,<sup>1,2</sup> Jianchen Dang,<sup>1,2</sup> Sibai Sun,<sup>1,2</sup> Longlong Yang,<sup>1,2</sup> Yunuan Wang,<sup>1,3</sup> Shushu Shi,<sup>1,2</sup> Jiongji He,<sup>1,2</sup> Zhanjun Zuo,<sup>1,2</sup> and Xiulai Xu<sup>1,2,4,\*</sup>

<sup>1</sup>Beijing National Laboratory for Condensed Matter Physics, Institute of Physics, Chinese Academy of Sciences, Beijing 100190, China

<sup>2</sup>CAS Center for Excellence in Topological Quantum Computation and School of Physical Sciences, University of Chinese Academy of Sciences, Beijing 100049, China

<sup>3</sup>Key Laboratory of Luminescence and Optical Information, Ministry of Education, Beijing Jiaotong University, Beijing 100044, China

<sup>4</sup>Songshan Lake Materials Laboratory, Dongguan, Guangdong 523808, China

(Received 11 March 2020; revised 13 May 2020; accepted 8 June 2020; published 16 July 2020)

We report high-resolution photocurrent (PC) spectroscopy of a single self-assembled InAs/GaAs quantum dot embedded in an  $n-i$  Schottky device in an applied vector magnetic field. The PC spectra of positively charged excitons ( $X^+$ ) and neutral excitons ( $X^0$ ) are obtained by two-color resonant excitation. With an applied magnetic field in the Voigt geometry, the double- $\Lambda$  energy-level structure of  $X^+$  and the dark states of  $X^0$  are observed clearly in the PC spectra. In the Faraday geometry, the PC amplitude of  $X^+$  decreases and is then quenched with increasing magnetic field, which provides a new way to determine the relative sign of the electron and hole  $g$ -factors. With an applied vector magnetic field, the electron and hole  $g$ -factor tensors of  $X^+$  and  $X^0$  are obtained. The anisotropy of the hole  $g$ -factors of both  $X^+$  and  $X^0$  is larger than that of the electron  $g$ -factors.

DOI: 10.1103/PhysRevApplied.14.014049

## I. INTRODUCTION

Electron and hole spins in semiconductor materials have long been considered as building blocks in quantum information processing and quantum computation [1]. Three-dimensionally confined quantum dots (QDs) provide a long coherence time for spin states, allowing the manipulation of single spin states [2–4]. During coherent control of spins in QDs, a magnetic field is usually used to modulate the properties of the spins and energy levels [5,6]. The  $g$ -factor, a very important parameter describing the coupling of spins to a fixed magnetic field in a QD [7,8], has been intensively studied in various systems. Generally, the  $g$ -factor shows anisotropy in different directions, and can be described as a  $g$ -factor tensor. Some efforts have been made to characterize the  $g$ -factor of excitons [9–11] and the  $g$ -factor tensor of confined carriers in QDs [12–16] by optical methods. In self-assembled QDs, the electron and hole  $g$ -factors are related to the size, shape, and composition [17,18], and can be tuned by an external field [19–24]. Additionally, the  $g$ -factors usually vary for different excitons due to Coulomb interactions [7]. However, there

have been few systematic studies of the electron and hole  $g$ -factor tensors of different excitons [25,26], which limits the possibility of a full description of the electronic properties of different excitons in single QDs.

Photocurrent (PC) spectroscopy of a single QD embedded in a diode has been proved an effective way to read out charge [27] and spin [28,29] information from a single QD directly, with high detection efficiency [30]. Compared with photoluminescence (PL) induced by nonresonant pumping, PC spectroscopy has a higher resolution when performed with continuous-wave (CW) resonant pumping, and can be used in coherent control with pulsed pumping [31–36]. On the other hand, the detection of the PC signal can be done without the need to filter out the pumping laser as is necessary in the case of resonant fluorescence, which is convenient for research on spin properties. In contrast, for resonant fluorescence, a cross-polarization configuration is usually constructed to eliminate the resonant laser background [37,38], which limits the extraction of the polarized signal for the purpose of obtaining spin information.

In this paper, we report on  $g$ -factor tensors of positively charged excitons  $X^+$  and neutral excitons  $X^0$  in a single self-assembled InAs/GaAs QD obtained through

\*xlxu@iphy.ac.cn

high-resolution PC spectroscopy in vector magnetic fields. The QDs are embedded in the intrinsic region of an *n-i* Schottky diode with a two-dimensional electron gas (2DEG) beneath. Two-color CW narrow-bandwidth (approximately 1 MHz) lasers are used to perform high-resolution PC measurement on  $X^+$ . With an applied vector magnetic field,  $X^+$  and  $X^0$  show Zeeman splitting and dark exciton states. The electron and hole *g*-factor tensors of  $X^+$  and  $X^0$  are obtained from the PC spectra. In addition, the quenching of the PC signal of  $X^+$  in a large magnetic field in the Faraday geometry reveals the opposite signs of the electron and hole *g*-factors. The hole *g*-factors show a larger anisotropy than the electron *g*-factors for both  $X^+$  and  $X^0$ , revealing that the hole *g* tensor is more sensitive to the geometry of the QD. This paper shows that PC spectroscopy is an effective and convenient way to characterize *g*-factors with high resolution.

## II. EXPERIMENTAL DETAILS

An *n-i* Schottky device is designed and fabricated for performing PC measurements on single QDs. A schematic diagram of the device is shown in Fig. 1(a). The Schottky contact is formed by evaporating a 10-nm semitransparent titanium layer onto the surface, followed by an Al mask with apertures of about 1–3  $\mu\text{m}$  to isolate single QDs. A 2DEG formed by a Si- $\delta$ -doped GaAs layer (doping density  $5 \times 10^{12} \text{ cm}^{-2}$ ), which serves as the Fermi sea of electrons in the device, is connected to Cr/Au bond pads on top of an alloyed (Au, Ge)Ni ohmic contact layer [39,40]. To enhance the photon collection efficiency, a distributed Bragg reflector (DBR) consisting of 13 pairs of Al<sub>0.94</sub>Ga<sub>0.06</sub>As(67 nm)/GaAs(71 nm) is grown at the bottom of the structure [41,42]. The vertical electric field that can be applied to the QDs is given by  $F = (V_i - V_b)/d$ , where  $V_i$  is the built-in potential (0.74 V for this device),  $V_b$  is the applied bias voltage, and  $d$  is the distance between the Schottky contact and the 2DEG. Further details of the design and fabrication of the device can be found in Ref. [43].

To perform resonant excitation of the QDs, two tunable narrow-bandwidth (approximately 1 MHz) external-cavity diode lasers in the Littrow configuration are provided. The nonresonant PL measurement is excited by a 650-nm semiconductor laser. A confocal microscope objective with a large numerical aperture of 0.82 is used to perform micro-PL and PC measurements on single QDs. The PL signals are collected and dispersed through a 0.55-m spectrometer with a spectral resolution of about 60  $\mu\text{eV}$ . To perform polarization-resolved PL and PC measurements, halfwave plates and polarizers are added to the pumping and collection paths. For all the measurements presented in this paper, the device is maintained at 4.2 K on an xyz piezoelectric stage in a helium-gas exchange cryostat equipped with superconducting magnets to supply a vector

magnetic field of up to 4 T. A semiconductor analyzer with a high current resolution (10 fA) is used for the electrical measurements.

## III. RESULTS AND DISCUSSION

The PC spectra are obtained through resonant excitation of  $X^0$  and  $X^+$ . Firstly, the  $X^0$  is excited resonantly by a laser with energy  $E_L^0$ . The electron tunnels out of the QD preferentially due to its small effective mass, leaving a single heavy hole in the valence band, as shown in Fig. 1(b). Through pumping-power-dependent PC measurements, an analysis of the linewidth gives the typical electron tunneling time as several picoseconds, with a tunnel barrier height of about 60 meV [44,45]. The hole then tunnels out of the QD and contributes to the  $X^0$  PC signal, as shown by the black solid points in Fig. 1(c). In this QD, the hole tunneling time is measured as 3.96 ns, with a tunnel barrier height of 45.51 meV, by an analysis of the PC amplitude in a power-dependent measurement [46]. Meanwhile, if a second laser with energy  $E_L^+$ , resonant with  $X^+$ , is applied to the QD, the hole state  $|h\rangle$ , as an initial state, can be excited to  $X^+$ . After the electron tunnels out of the QD, one hole tunnels out first, due to the enhanced tunneling rate induced by the Coulomb repulsion between the two holes. Here, the Coulomb interaction lowers the tunnel barrier to 37.46 meV and accelerates the hole tunneling to about 30 times faster, with a tunneling time of 0.14 ns [46]. The remaining hole can either tunnel out of the QD or be excited to  $X^+$  again. Here, linearly polarized lasers are used to excite both  $X^0$  and  $X^+$ . So, all the spin states of  $X^+$  and  $X^0$  can be excited equally. No matter which hole spin state it is in, the system can be repumped to  $X^+$  again, as shown in the right panel of Fig. 1(b). The Coulomb-induced acceleration of hole tunneling and the reuse of the hole state contribute to the much larger PC signal of  $X^+$  than of  $X^0$ , as shown in Fig. 1(c). A detailed discussion of this mechanism can be found in a previous publication [46]. If the excitation energy  $E_L^+$  is tuned, the  $X^+$  PC peaks appear at different bias voltages accordingly, as shown by the colored curves in Fig. 1(c). Through a simple subtraction under conditions of relatively low pumping power, the pure  $X^+$  PC spectra are obtained, as shown in Fig. 1(d). Compared with  $X^0$ , the PC spectrum of  $X^+$  has a narrow linewidth due to the Coulomb attraction prolonging the electron tunneling time. The linewidth of the  $X^+$  peaks in the PC spectra in Fig. 1(d) are all about 15  $\mu\text{eV}$ , which offers a higher resolution than for  $X^0$ , with a linewidth of 230  $\mu\text{eV}$ .

The variation of the exciton transition energy with the electric field (or bias voltage) is described by the Stark shift, with an expression  $E(F) = E(0) + pF + \beta F^2$ , where  $E(0)$  is the transition energy without the external electric field,  $p$  is the permanent dipole moment, and  $\beta$  is the polarizability of the electron-hole wave function.

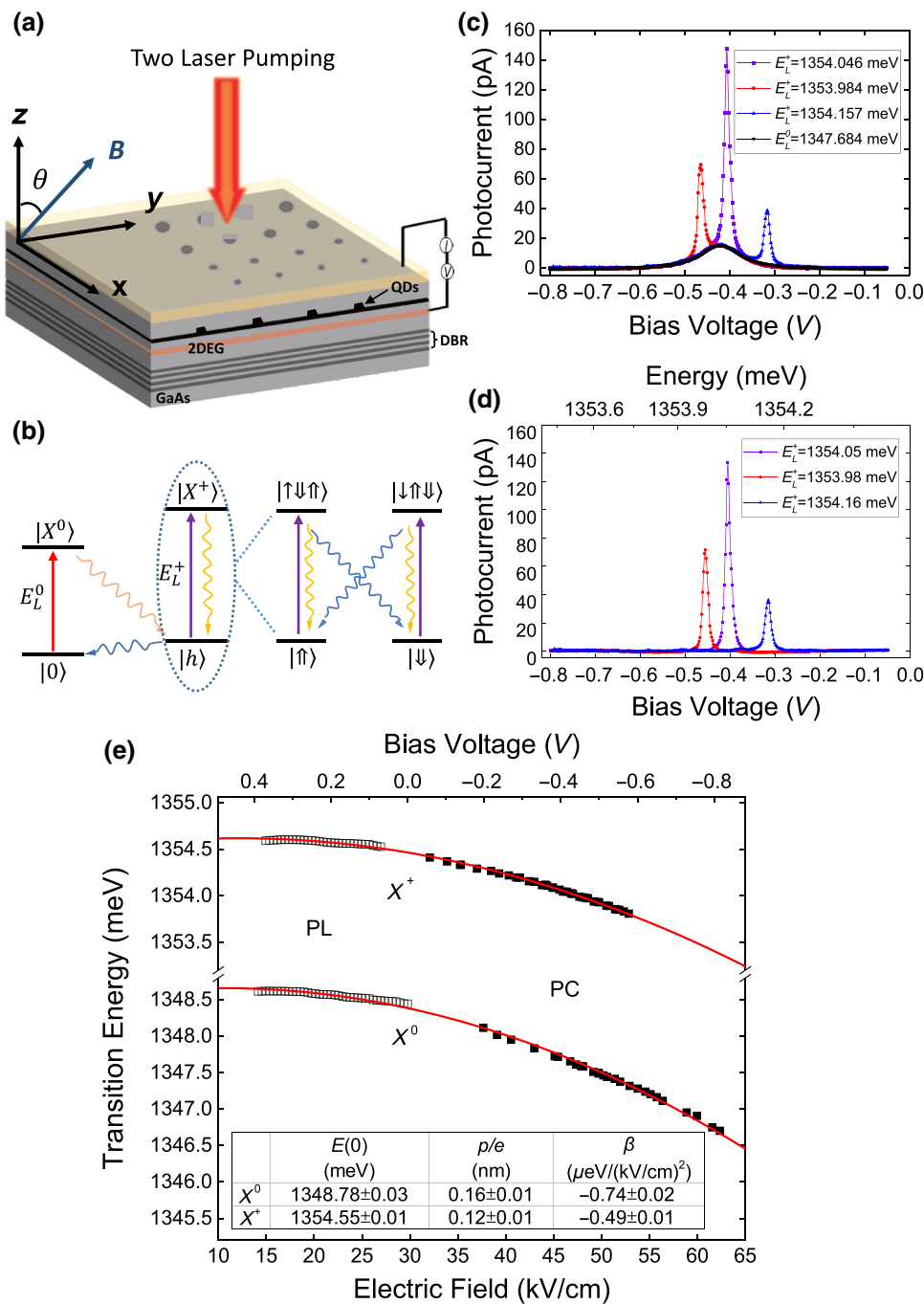


FIG. 1. (a) Schematic diagram of the  $n$ - $i$  Schottky device and PC measurement in a vector magnetic field. Here,  $\theta$  is the angle between the magnetic field ( $B$ ) and the growth axis of the QDs ( $z$  direction). (b) Two-color excitation scheme used for the  $X^+$  PC measurements. The solid and wavy arrows represent the excitation and tunneling processes, respectively, of carriers. (c) PC spectra of  $X^0$  and  $X^+$  under two-color excitation. The black solid points represent the pure  $X^0$  PC spectrum with  $E_L^0 = 1347.684$  meV. The red, purple, and blue solid points represent the measured PC spectra of  $X^+$  for different energies of the second laser,  $E_L^+$ . (d) Subtracted PC spectra of  $X^+$  for different energies of the second laser. The top  $x$  axis represents the Stark shift of  $X^+$ . (e) Stark shifts of  $X^0$  and  $X^+$  as a function of the electric field and the bias voltage obtained from the single-QD PL (empty squares) and PC (solid squares) spectra. The solid red lines represent quadratic fits to the quantum confined Stark effect for  $X^0$  and  $X^+$ . The fitting parameters for  $E(0)$ ,  $p$ , and  $\beta$  are given in the table in the inset.

By tuning the pumping-laser wavelength, a series of PC spectra are obtained for  $X^0$  and  $X^+$ . The Stark shifts obtained by combining the series of PL and PC spectra are shown in Fig. 1(e). From the results of fitting shown in the inset of Fig. 1(e), the functions relating the electric field (or bias voltage) applied to the QD and the transition energies of  $X^0$  and  $X^+$  can be determined precisely. Using the functions determined, the corresponding energy of  $X^+$  can be derived, as shown on the top  $x$  axis in Fig. 1(d). Furthermore, the fitting parameters in Fig. 1(e) can also

provide the dipole moment and polarizability of  $X^0$  and  $X^+$  precisely [47].

In order to obtain the electron and hole  $g$ -factor tensors, the PC spectrum in a magnetic field in the Voigt geometry is first measured. When a magnetic field is applied perpendicular to the sample growth direction ( $z$  direction), namely, in the Voigt geometry, the spin degeneracy of electrons and holes is lifted, which induces a Zeeman splitting of the  $|X^+\rangle$  and  $|h\rangle$  states and forms a double- $\Lambda$  structure, as presented in Fig. 2(a). Generally, due to the large

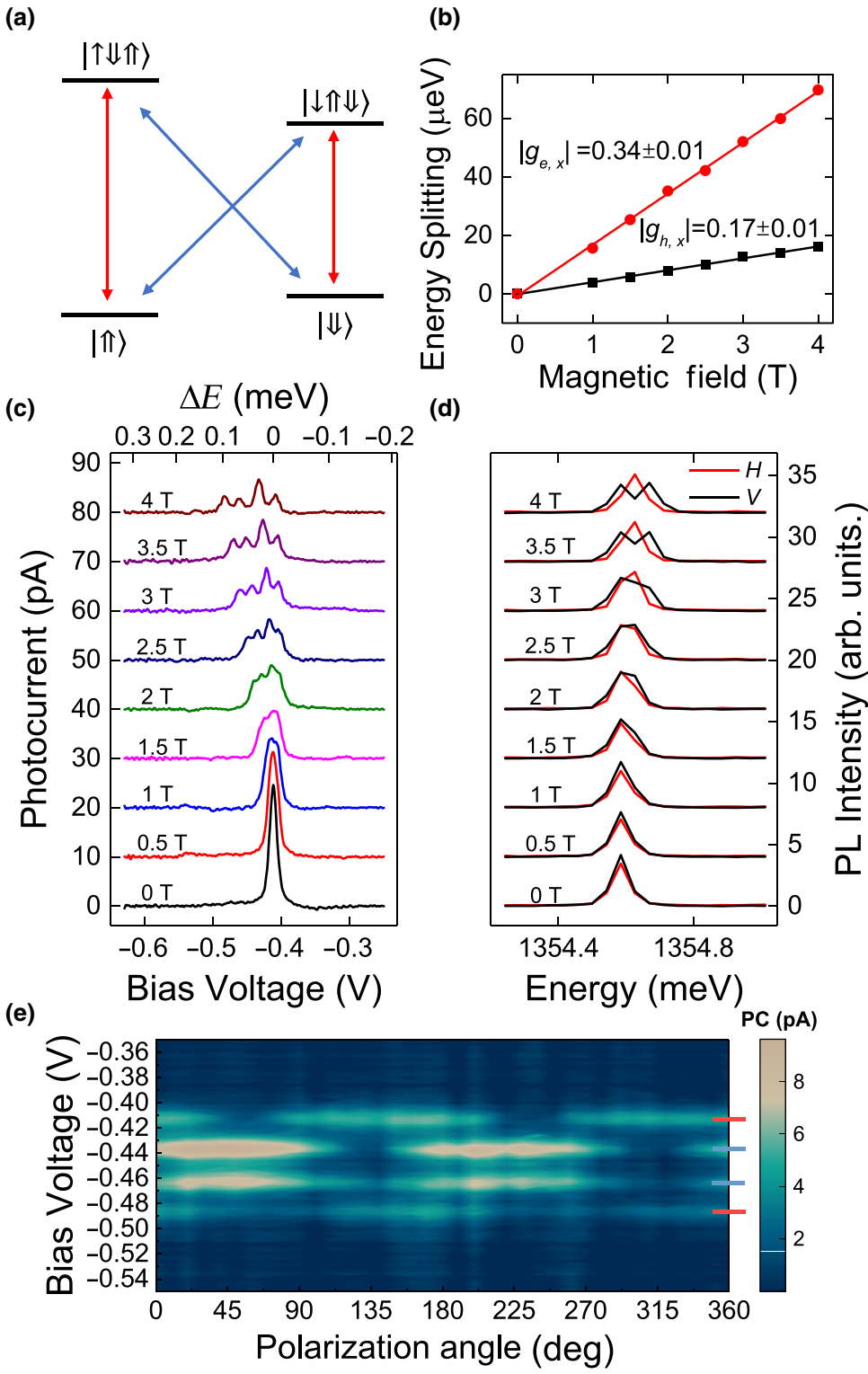


FIG. 2. (a) Energy-level structure of  $X^+$  in a magnetic field. Here, the two inner transitions (blue solid arrows), with an angular momentum of  $M = \pm 2$ , are dark-state transitions. The two outer transitions (red solid arrows), with  $M = \pm 1$ , are bright-state transitions. (b) Zeeman splitting of  $|X^+\rangle$  and  $|h\rangle$  states in the Voigt geometry. (c) PC spectra of  $X^+$  in a magnetic field from 0 to 4 T in the Voigt geometry. The spectra are shifted for clarity. (d) Polarization-resolved PL spectra of  $X^+$  in a magnetic field from 0 to 4 T in the Voigt geometry. The spectra are shifted for clarity. (e) Polarization-resolved PC spectra of  $X^+$  in a 4-T Voigt magnetic field, where the short blue and red lines on the right are guides to the eye for the dark and bright states, respectively.

strain-induced splitting between heavy- and light-hole states, only heavy holes ( $|↑\uparrow\rangle$  or  $|↓\downarrow\rangle$ ) with an angular momentum  $J_{h,z} = \pm 3/2$  are considered for self-assembled QDs [48,49]. For an electron ( $|↑\downarrow\rangle$  or  $|↓\uparrow\rangle$ ) at the bottom of the conduction band, the total angular momentum is equal to the spin momentum  $S_{e,z} = \pm 1/2$ . Therefore, the

total angular momentum of an electron-hole pair can be defined as  $M = J_{h,z} + S_{e,z}$ . Transitions with  $M = \pm 1$  satisfy the selection rules and are defined as bright states, while transitions with  $M = \pm 2$  cannot couple to the light field and are defined as dark states. For  $X^+$ , the value of  $M$  can be defined as the change between the initial

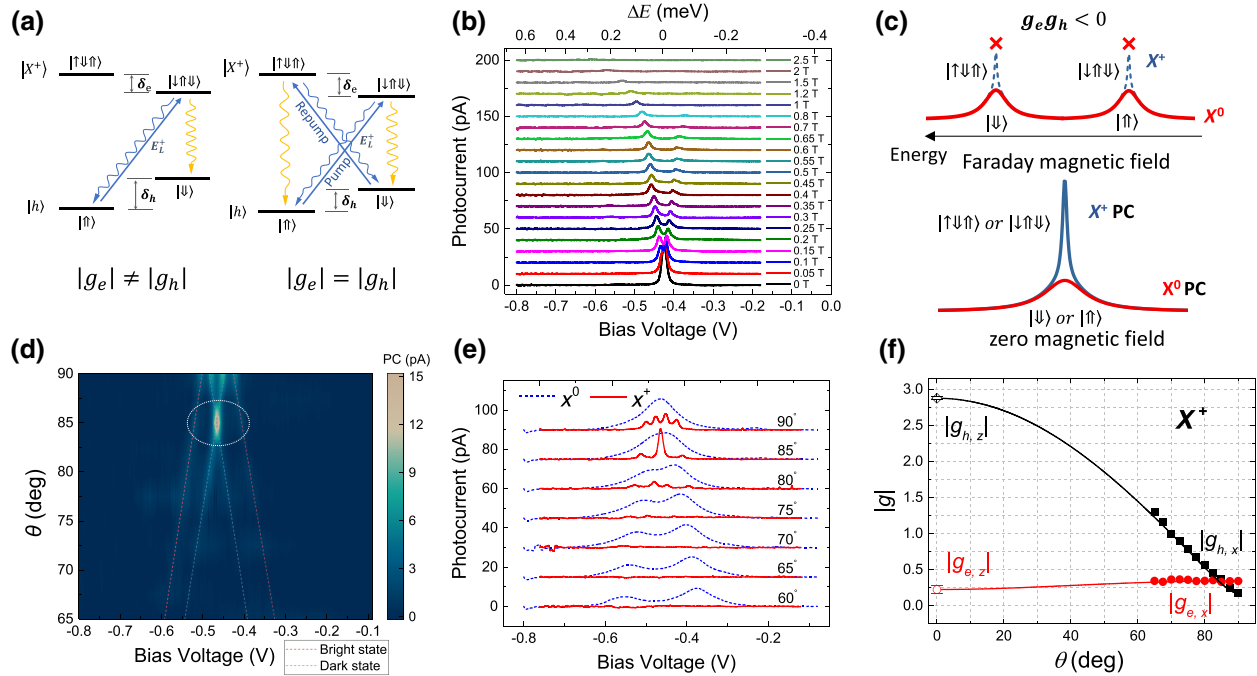


FIG. 3. (a) Schematic diagram of the carrier transitions and decays in  $X^+$  in a magnetic field with  $|g_e| \neq |g_h|$  (left panel) and  $|g_e| = |g_h|$  (right panel). The solid and wavy lines represent the excitation and tunneling processes, respectively. (b) PC spectra of  $X^+$  in a magnetic field in the Faraday geometry from 0 to 2.5 T. The top  $x$  axis represents the energy shift compared with the  $X^+$  transition energy at zero magnetic field. The spectra are shifted for clarity. (c) Schematic diagram of  $X^+$  and  $X^0$  PC spectra in zero magnetic field (bottom panel) and a Faraday magnetic field (top panel) under the condition  $g_e g_h < 0$ . Here, the red and blue curves represent the PC spectra of  $X^0$  and  $X^+$ , respectively. (d) Magneto-PC mapping of  $X^+$  in a 4-T vector magnetic field at angles from  $90^\circ$  to  $65^\circ$ . Here, the red and blue dashed lines are guides to the eye for the bright- and dark-state transitions, respectively, of  $X^+$ . (e) PC spectra of  $X^+$  and  $X^0$  in a 4-T vector magnetic field with  $\theta$  from  $90^\circ$  to  $60^\circ$ . The red solid curves are the PC spectra of  $X^+$ , and the blue dashed curves are the PC spectra of  $X^0$ . (f) Electron and hole  $g$ -factors of  $X^+$  as a function of the angle  $\theta$ . The solid dots are the extracted electron and hole  $g$ -factors, with error bars of about 0.02. The red and black dots at  $\theta = 0^\circ$  show  $|g_{e,z}|$  and  $|g_{h,z}|$  derived by fitting the extracted data to Eq. (1) (solid curves) under the condition  $|g_{e,z}| + |g_{h,z}| = 3.10 \pm 0.02$ .

and final states. Here, the transitions  $\left|\uparrow\downarrow\uparrow\right\rangle \leftrightarrow \left|\uparrow\uparrow\right\rangle$  and  $\left|\downarrow\uparrow\downarrow\right\rangle \leftrightarrow \left|\downarrow\downarrow\right\rangle$  [red arrows in Fig. 2(a)] have an angular momentum of  $M = \pm 1$ , satisfy the selection rules, and are defined as bright states, while the transitions  $\left|\uparrow\downarrow\uparrow\right\rangle \leftrightarrow \left|\downarrow\downarrow\right\rangle$  and  $\left|\downarrow\uparrow\downarrow\right\rangle \leftrightarrow \left|\uparrow\uparrow\right\rangle$  (blue arrows), with an angular momentum of  $M = \pm 2$ , are usually defined as dark states and are optically forbidden. However, the magnetic field in the Voigt geometry destroys the rotation symmetry and couples the bright and dark states, resulting in optical access and linear polarization of the dark states.

Figure 2(c) shows the corresponding PC spectra of  $X^+$ , with the appearance of the double- $\Lambda$  structure; the top  $x$  axis represents the energy shift with respect to 0 T. Here, the excitation laser is linearly polarized, with the polarization direction along  $45^\circ$  with respect to the applied Voigt magnetic field, so as to excite the four transitions of  $X^+$  equally. Note that because of the fixed energy of the pumping laser, the energy level of  $X^+$  is tuned lower to match the laser energy, with an additional energy shift induced by the diamagnetic effect and the Zeeman splitting. As a

result, the peaks of the PC spectra move in the direction of negative bias voltage (high electric field) at a high magnetic field [50]. Here, because the giant enhancement of the  $X^+$  PC caused by the reuse of the hole state is destroyed by the magnetic field, the PC amplitudes in Fig. 2(c) decrease with increasing magnetic field. In order to illustrate this process, we first assume that the laser excites the transition  $\left|\uparrow\uparrow\right\rangle \rightarrow \left|\downarrow\uparrow\downarrow\right\rangle$ , as shown in the left panel of Fig. 3(a). After one electron-hole pair in  $X^+$  tunnel out, the system decays to  $\left|\uparrow\uparrow\right\rangle$  or  $\left|\downarrow\downarrow\right\rangle$ . If it decays to  $\left|\uparrow\uparrow\right\rangle$ , the laser can reuse the hole state and excite the system back to  $\left|\downarrow\uparrow\downarrow\right\rangle$ , while if it decays to  $\left|\downarrow\downarrow\right\rangle$ , due to the detuning between the laser energy and the transition energies from  $\left|\downarrow\downarrow\right\rangle$  to  $X^+$ , the system stays in this state until the hole tunnels out. As a result, the enhancement mechanism is destroyed because of the Zeeman splitting, which causes a decrease in the  $X^+$  PC amplitude in the magnetic field. In contrast to the PC spectra, we cannot distinguish any splitting in the nonresonant-excitation PL spectra, but only a linewidth broadening. Even with polarization-resolved PL measurements, only three peaks can be observed at 4 T, as shown in

TABLE I. Values of  $g$ -factors and anisotropy factors for both positively charged excitons  $X^+$  and neutral excitons  $X^0$ .

$g$ -factor	$X^+$	$X^0$
$ g_{e,x} $	$0.34 \pm 0.01$	$0.15 \pm 0.03$
$ g_{h,x} $	$0.17 \pm 0.01$	$0.59 \pm 0.10$
$ g_{e,z} $	$0.22 \pm 0.05$	$0.26 \pm 0.08$
$ g_{h,z} $	$2.88 \pm 0.02$	$2.83 \pm 0.15$
$P_{e,x-z}$	$(17.91 \pm 0.11)\%$	$(26.82 \pm 0.34)\%$
$P_{h,x-z}$	$(88.55 \pm 0.02)\%$	$(90 \pm 0.17)\%$

Fig. 2(d). Clearly, PC spectroscopy offers better resolution than does PL in our experiment.

The polarization-resolved PC spectra of  $X^+$  in a 4-T Voigt-configuration magnetic field are shown in Fig. 2(e), which reveals the orthogonal linear polarizations of the four transitions of  $X^+$  clearly and proves the formation of the double- $\Lambda$  energy-level structure again. The two outer PC peaks, with polarizations orthogonal to the Voigt magnetic field, marked by short red lines, are the transitions labeled with red arrows in Fig. 2(a), while the two inner PC peaks, marked by short blue lines, are the corresponding emissions of the two diagonal transitions labeled with blue arrows in Fig. 2(a), which have polarizations perpendicular to that of the two outer transitions. Through Lorentzian fitting of the PC peaks in Fig. 2(c), the splittings of  $|X^+\rangle$  and  $|h\rangle$  as a function of the magnetic field in the Voigt geometry are extracted, as shown by the red and black dots in Fig. 2(b). For this QD, the in-plane  $g$ -factors of electrons and holes are  $|g_{e,x}| = 0.34 \pm 0.01$  and  $|g_{h,x}| = 0.17 \pm 0.01$ , respectively.

To determine the  $z$  component of the electron and hole  $g$ -factor tensors, measurements of the PC spectra are performed with a magnetic field in both the Faraday geometry and an intermediate geometry between the Faraday and Voigt geometries, as shown in Fig. 3. In the Faraday geometry, i.e., with the magnetic field along the  $z$  direction, the PC spectra of  $X^+$  split into two peaks with opposite circular polarizations, as shown in Fig. 3(b). The observed Zeeman splitting is determined by the electron and hole  $g$ -factors, which can be expressed as  $\Delta E_{\text{Zeeman}} = \mu_B (|g_{e,z} - g_{h,z}|)B$ . By extracting the Zeeman splitting from Fig. 3(b), the exciton  $g$ -factor  $|g_{e,z} - g_{h,z}|$  is deduced as  $3.10 \pm 0.02$ . For the same reason as in the case of the Voigt geometry, the PC amplitude is weakened with an increase in the magnetic field. When the magnetic field is above 1.5 T, the PC amplitude starts to become quenched, which implies opposite signs of the electron and hole  $g$ -factors. To explain this phenomenon, we need to consider the case of zero magnetic field first. At zero magnetic field, the PC spectrum of  $X^0$  offers a hole background after the tunneling of an electron. The red solid curve in the bottom panel of Fig. 3(c) represents the hole background, with the same probabilities of spin-up and spin-down holes.

With the second laser, of energy  $E_L^+$ , on, the two-color excitation excites the system to  $X^+$ , as shown by the blue solid curve in the bottom panel of Fig. 3(c). This time, due to the superposition of hole backgrounds of different spins, there is no need to consider spin selection. In contrast, in a magnetic field in the Faraday geometry, due to the large  $g$ -factor of holes, the hole background offered by  $X^0$  splits into two peaks when the magnetic field is above 1.5 T, as shown by the red solid curve in the top panel in Fig. 3(c). Here, for better interpretation, we assume that the hole background on the high- (low-)energy side provides holes with spin down,  $|\Downarrow\rangle$  (spin up,  $|\Uparrow\rangle$ ). If the sign of the electron  $g$ -factor is opposite, then  $X^+$  has a state  $|\uparrow\Downarrow\Uparrow\rangle$  ( $|\downarrow\Uparrow\Downarrow\rangle$ ) at the corresponding energy, as shown by the blue dashed curves in the top panel in Fig. 3(c). However, due to the selection rule, this transition  $|\Downarrow\rangle \longleftrightarrow |\uparrow\Downarrow\Uparrow\rangle$  ( $|\Uparrow\rangle \longleftrightarrow |\downarrow\Uparrow\Downarrow\rangle$ ), with angular momentum  $M = \pm 2$ , is forbidden in a Faraday magnetic field, leading to the PC amplitude of  $X^+$  becoming quenched in a magnetic field of up to 1.5 T. Therefore, the two-color excitation scheme for  $X^+$  provides a way to get the relative signs of the electron and hole  $g$ -factors, and the  $g$ -factor of  $X^+$  can be represented as  $|g_{e,z}| + |g_{h,z}|$  through the opposite signs of  $g_{e,z}$  and  $g_{h,z}$ . Note that due to the larger electric field in the higher-energy branch, the PC amplitude is larger than that for the lower-energy branch in Fig. 3(b). As a result, the PC signals are quenched faster in the lower-energy branch.

The PC spectra in a vector magnetic field are recorded as a function of  $\theta$ , as defined in Fig. 1(a). A color plot of the PC spectra of  $X^+$  in a 4-T vector magnetic field with  $\theta$  ranging from  $90^\circ$  to  $65^\circ$  is shown in Fig. 3(d). As the angle  $\theta$  decreases, i.e., the magnetic field changes from the Voigt to the Faraday geometry, the splitting of the outer transitions increases and the lines of the two inner transitions cross each other. An interesting feature is the enhancement of the PC of the inner transitions at  $\theta = 85^\circ$ . This enhancement can be ascribed to the repumping of the hole state [51], as shown in the schematic diagram in the right panel of Fig. 3(a). Unlike the case for  $|g_e| \neq |g_h|$  [left panel of Fig. 3(a)], the absolute value of the electron  $g$ -factor is equal to that of the hole  $g$ -factor at  $\theta = 85^\circ$ , resulting in the same energy of diagonal transitions. Therefore, a laser resonant with both diagonal transitions can repump the hole state to the  $X^+$  state, no matter which spin state ( $|\Downarrow\rangle$  or  $|\Uparrow\rangle$ ) the hole state is in. Thus the reuse of the hole state can be restored, and the PC amplitude becomes much larger, as shown clearly in Figs. 3(d) and 3(e). The PC amplitude becomes weaker as  $\theta$  decreases, for the same reason as in the case of a large Faraday magnetic field discussed before. As shown in Fig. 3(e), for  $\theta$  from  $90^\circ$  to  $60^\circ$ , the PC spectrum of  $X^0$  splits into two peaks (blue dashed lines). The forbidden transitions caused by the opposite signs of the electron and hole  $g$ -factors weaken the  $X^+$  PC amplitude (red solid lines) and eventually make it disappear when the PC spectrum of  $X^0$  is totally separated.

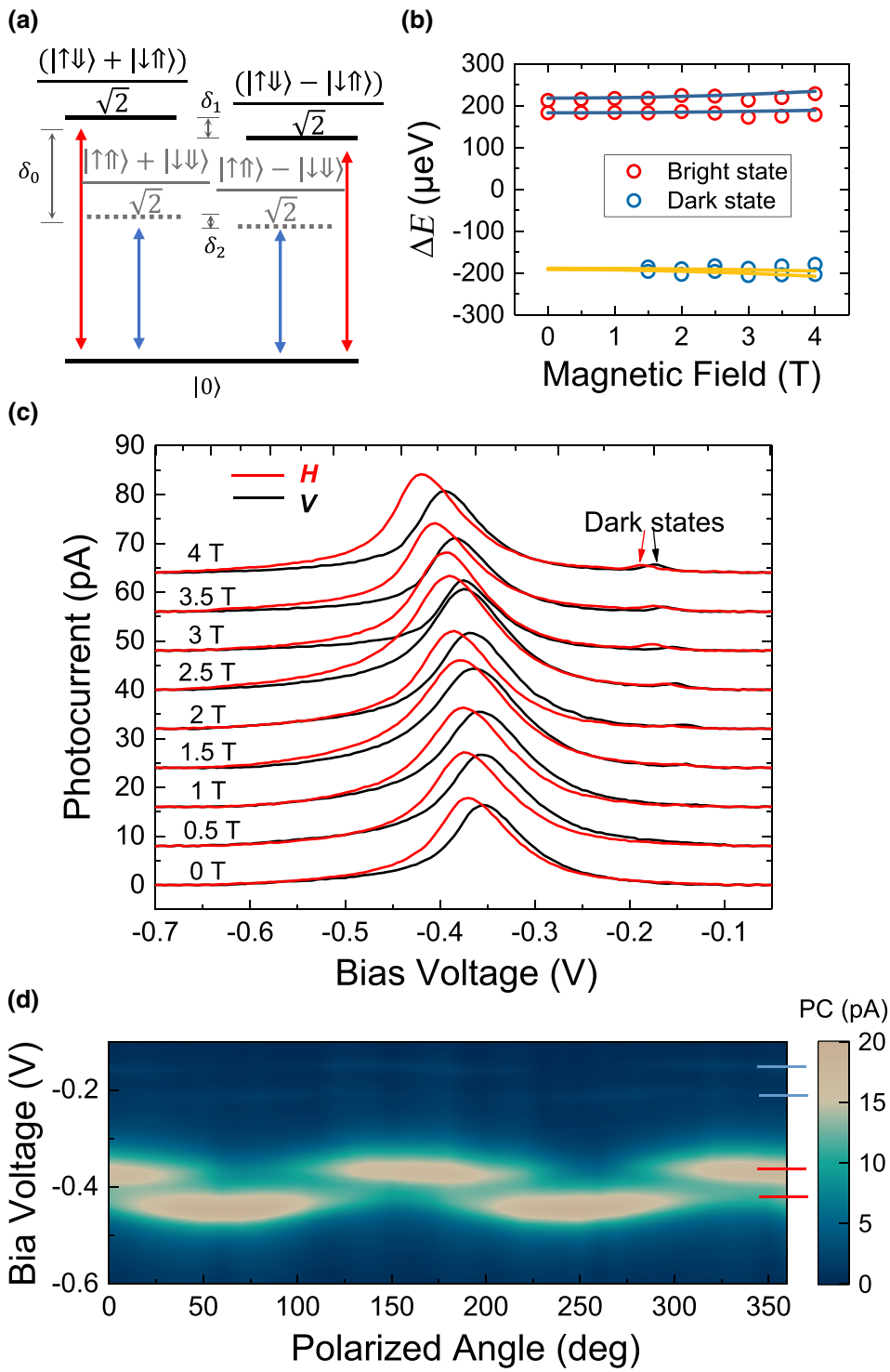


FIG. 4. (a) Energy-level structure of  $X^0$  in a magnetic field in the Voigt geometry. Here,  $\delta_0$  represents the energy difference between the bright and the dark states, and  $\delta_1$  and  $\delta_2$  represent the FSS of the bright and dark states, respectively; these are referred to as the exchange parameters. (b) Zeeman splitting of bright and dark states in a magnetic field in the Voigt geometry. The diamagnetic shift is deduced. Here, the circles are the extracted data, and the solid curves are fitted results with consideration of the exchange parameters  $\delta_0$ ,  $\delta_1$ , and  $\delta_2$ . (c) Polarization-resolved PC spectra of  $X^0$  in magnetic fields from 0 to 4 T in the Voigt geometry. The spectra are shifted for clarity. (d) Linear-polarization-resolved PC spectra at 4 T in the Voigt geometry. The short blue and red lines are guides to the eye for the dark and bright states of  $X^0$ .

The behavior of  $X^+$  in a vector magnetic field can be described by the  $g$ -factors of electrons and holes as a function of  $\theta$ :

$$g_{e,h}(\theta) = \sqrt{(g_{e,h,x} \cos \theta)^2 + (g_{e,h,z} \sin \theta)^2}. \quad (1)$$

The extracted  $g$ -factors of electrons and holes can be fitted according to Eq. (1), as shown in Fig. 3(f). Here,

the  $g$ -factor of  $X^+$  ( $|g_{e,z}| + |g_{h,z}| = 3.10 \pm 0.02$ ) is also used as a parameter to fit the  $g$ -factor tensor in Fig. 3(f). The hole  $g$ -factor shows a larger anisotropy than the electron  $g$ -factor, consistent with other studies [16,52]. The anisotropy factors of the electron and hole  $g$ -factors can be described as  $P_{e,x-z} = (g_{e,x} - g_{e,z})/(g_{e,x} + g_{e,z}) = (17.91 \pm 0.01)\%$  and  $P_{h,x-z} = (g_{h,x} - g_{h,z})/(g_{h,x} + g_{h,z}) = (88.55 \pm 0.02)\%$ , as shown in Table I. This can be ascribed to

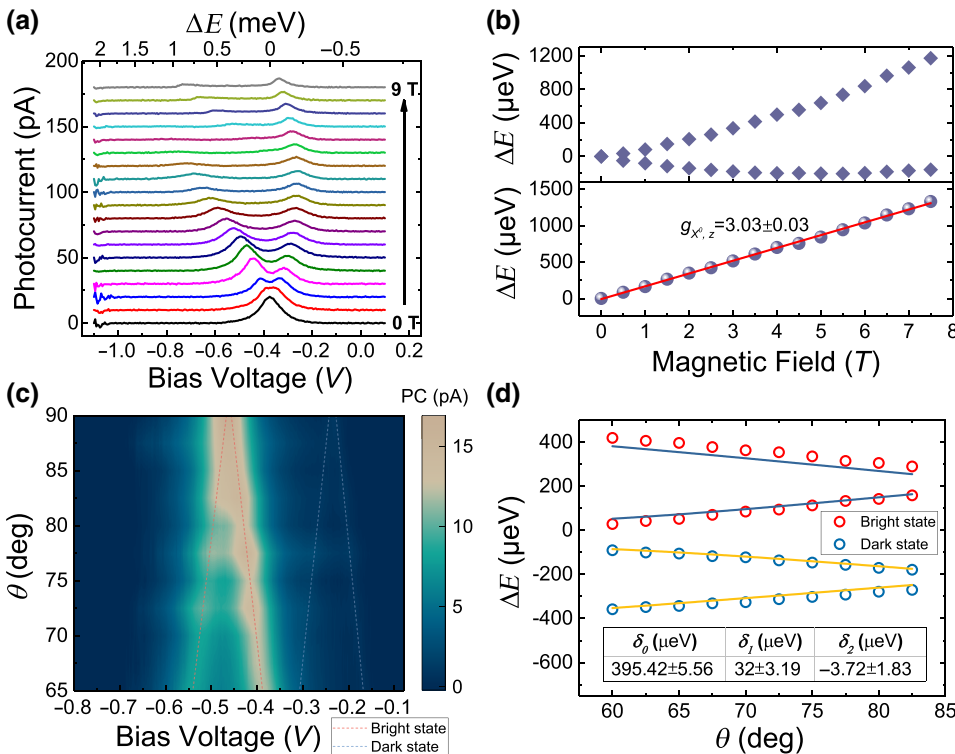


FIG. 5. (a) PC spectra of  $X^0$  in a magnetic field from 0 to 9 T in the Faraday geometry. The top  $x$  axis represents the energy shift compared with the  $X^+$  transition energy at zero magnetic field. The spectra are shifted for clarity. (b) Top panel: energy of  $X^0$  extracted from part (a) as a function of the magnetic field, offset by the mean at 0 T. Bottom panel: Zeeman splitting of  $X^0$ , from which the  $g$ -factor is derived as  $3.03 \pm 0.03$ . (c) Magneto-PC mapping of  $X^0$  in a 4-T vector magnetic field. The red and blue dashed lines represent the bright and dark states, respectively. (d) Fitting results for the splitting of  $X^0$  in a vector magnetic field. The circles represent the extracted data for the four transitions in part (c) without the diamagnetic shift. The solid curves show the fitted results. The fitted exchange parameters are shown in the inset table.

the anisotropic shape of the QD, leading to different spatial real-space wave-function distributions and to nonzero orbital momenta carried by the hole states [53–55]. Previous studies using coherent population trapping by resonant fluorescence spectroscopy have measured the  $g$ -factors of  $X^+$  with very high resolution [56,57], but they also needed sophisticated device-fabrication and experimental techniques. Here, the use of PC spectroscopy provides a convenient way to investigate the spin properties.

Differently from  $X^+$ , due to the electron-hole exchange interaction and the asymmetry of the QD structure, the energy degeneracy of the states of the neutral exciton  $X^0$  without a magnetic field is lifted by the fine-structure splitting (FSS). A systematic description can be found in Ref. [49]. For an  $X^0$  consisting of an electron and a heavy hole, the exciton states  $|\uparrow\downarrow\rangle$  and  $|\downarrow\uparrow\rangle$  are mixed to form a new basis with total angular momentum  $M = \pm 1$ ,  $(|\uparrow\downarrow\rangle + |\uparrow\downarrow\rangle)/\sqrt{2}$  and  $(|\uparrow\downarrow\rangle - |\uparrow\downarrow\rangle)/\sqrt{2}$ , which satisfy the selection rule and are defined as the bright states. The exciton states  $|\uparrow\uparrow\rangle$  and  $|\downarrow\downarrow\rangle$  are mixed to form  $(|\uparrow\uparrow\rangle + |\downarrow\downarrow\rangle)/\sqrt{2}$  and  $(|\uparrow\uparrow\rangle - |\downarrow\downarrow\rangle)/\sqrt{2}$ , with total angular momentum  $M = \pm 2$ ; these are forbidden by the selection rule and are defined as the dark states, as shown in Fig. 4(a). Additionally, the mixing of the exciton states induces orthogonal linear polarizations, which enable us to distinguish the FSS by means of polarization-resolved PC spectra. The FSS of the bright states,  $\delta_1$ , is usually larger than that of the dark states,  $\delta_2$ . The energy difference between the bright states and dark states,  $\delta_0$ , and the FSSs  $\delta_1$  and  $\delta_2$  of the bright and dark states are

collectively referred to as the exchange parameters, and are the vital parameters of  $X^0$ . To observe the dark states, a magnetic field in the Voigt geometry is applied, which can couple the bright and dark states and make the dark states optically accessible by destroying the rotational symmetry. We repeat the polarization-resolved PC measurements with magnetic fields from 0 to 4 T in the Voigt geometry, as shown in Fig. 4(c). As expected, the dark states emerge at 1.5 T [50]. The linear-polarization-resolved PC spectra at 4 T are shown in Fig. 4(d), with the short blue and red lines representing the dark and bright states, respectively; these spectra reveal the orthogonal linear polarizations clearly. The extracted energies of the bright and dark states are shown in Fig. 4(b), obtained by deducting the diamagnetic effect. But the fitting involves too many parameters, including the exchange parameters and the in-plane  $g$ -factors of electrons and holes. For more accuracy, we fit the data in combination with results in a Faraday magnetic field and in a vector magnetic field, as discussed below.

Measurements of the PC spectra of  $X^0$  in the Faraday geometry are performed, which show the Zeeman splitting and the diamagnetic effect clearly, as presented in Fig. 5(a). The  $g$ -factor of  $X^0$  is fitted as  $3.03 \pm 0.03$ , as shown in Fig. 5(b); this can be used as a more reliable parameter ( $g_{X^0,z} = |g_{e,z} + g_{h,z}|$ ) to fit other parameters. Next, PC spectra in a vector magnetic field of 4 T are measured, as shown in Fig. 5(c). For a small range of  $\theta$  from  $75^\circ$  to  $60^\circ$ , which corresponds to a large magnetic field in the Faraday geometry, the splittings of the bright and dark states

increase due to the larger  $g$ -factor in the Faraday geometry. On the other hand, the PC spectra of dark excitons become weaker because of the weaker coupling between dark and bright excitons in a small magnetic field in the Voigt geometry. We combine all the PC data for magnetic fields in different geometries and fit them together with the model presented in Ref. [49], as shown in Figs. 4(b) and 5(d). The exchange parameters and  $g$ -factors are shown in Fig. 5(d) and Table I, respectively. Because of the different Coulomb interactions, the  $g$ -factors have different values for  $X^0$  and  $X^+$ . Also, compared with  $X^+$ , the anisotropy factors of  $X^0$  for both electrons and holes are larger, which is due to the different contributions of heavy-hole-light-hole mixing in the compositions of the electronic states [58].

Note that the fitting results for  $X^0$  are not as good as those for  $X^+$ . There are many reasons for this. Firstly, the electron-hole exchange interaction and the existence of the FSS make the fitting of  $X^0$  more complicated. Secondly, the linewidth of the  $X^0$  PC spectrum is much broader than that for  $X^+$ , which also increases the uncertainties in the measurement and the fitting. For example, the splitting in a Voigt magnetic field cannot be distinguished directly. As a result, polarization-resolved measurements of PC spectra have to be performed, and these introduce more errors. Finally, the PC amplitude of dark states is very weak, and the splitting is small. So, the related fitting parameters have relatively larger errors. Nevertheless, PC spectroscopy of  $X^0$  still provides a method to identify the exchange parameters and  $g$ -factor tensors of electrons and holes.

#### IV. CONCLUSION

In conclusion, we measure the electron and hole  $g$  tensors of  $X^+$  and  $X^0$  in a single QD by high-resolution PC spectroscopy in a vector magnetic field. For  $X^+$ , the vertical and in-plane  $g$ -factors of electrons and holes are obtained precisely. The PC spectrum of  $X^+$  obtained by two-color excitation also illustrates the opposite signs of the electron and hole  $g$ -factors in the Faraday geometry, showing that PC spectroscopy provides a convenient way to investigate spin properties. Furthermore, a large PC enhancement is observed with a vector magnetic field when the electrons and holes have the same absolute value of the  $g$ -factor. The  $g$ -factors of  $X^0$ , as well as parameters related to the electron-hole exchange interaction, are also fitted through magneto-PC measurements. For both  $X^+$  and  $X^0$ , the hole  $g$ -factors show larger anisotropy than the electron  $g$ -factors. Our results prove that PC spectroscopy is a powerful tool to study QDs, and give an intuitive picture of the electron and hole  $g$ -factors of different excitons; this picture gives a full determination of the electronic properties of different excitonic states in QDs through PC spectroscopy.

#### ACKNOWLEDGMENTS

This work was supported by the National Natural Science Foundation of China under Grants No. 11934019, No. 61675228, No. 11721404, No. 51761145104, and No. 11874419; the Strategic Priority Research Program, the Instrument Development Project, and the Interdisciplinary Innovation Team of the Chinese Academy of Sciences under Grants No. XDB28000000 and No. YJKYYQ20180036; and the Key RD Program of Guangdong Province under Grant No. 2018B030329001. S. Wu and K. Peng contributed equally to this work.

- [1] D. P. DiVincenzo, in *Semiconductor Spintronics and Quantum Computation*, edited by D. D. Awschalom, D. Loss, and N. Samarth (Springer Berlin Heidelberg, Berlin, Heidelberg, 2002), pp. 221–227.
- [2] D. Loss and D. P. DiVincenzo, Quantum computation with quantum dots, *Phys. Rev. A* **57**, 120 (1998).
- [3] P. Chen, C. Piermarocchi, L. J. Sham, D. Gammon, and D. G. Steel, Theory of quantum optical control of a single spin in a quantum dot, *Phys. Rev. B* **69**, 075320 (2004).
- [4] D. Press, T. D. Ladd, B. Zhang, and Y. Yamamoto, Complete quantum control of a single quantum dot spin using ultrafast optical pulses, *Nature* **456**, 218 (2008).
- [5] L. Gaudreau, G. Granger, A. Kam, G. C. Aers, S. A. Stoudenikin, P. Zawadzki, M. Pioro Ladrière, Z. R. Wasilewski, and A. S. Sachrajda, Coherent control of three-spin states in a triple quantum dot, *Nat. Phys.* **8**, 54 (2012).
- [6] D. D. Awschalom, L. C. Bassett, A. S. Dzurak, E. L. Hu, and J. R. Petta, Quantum spintronics: Engineering and manipulating atom-like spins in semiconductors, *Science* **339**, 1174 (2013).
- [7] A. J. Bennett, M. A. Pooley, Y. Cao, N. Sköld, I. Farmer, D. A. Ritchie, and A. J. Shields, Voltage tunability of single-spin states in a quantum dot, *Nat. Commun.* **4**, 1522 (2013).
- [8] Y. Kato, R. C. Myers, D. C. Driscoll, A. C. Gossard, J. Levy, and D. D. Awschalom, Gigahertz electron spin manipulation using voltage-controlled  $g$ -tensor modulation, *Science* **299**, 1201 (2003).
- [9] J. Pingenot, C. E. Pryor, and M. E. Flatté, Method for full Bloch sphere control of a localized spin via a single electrical gate, *Appl. Phys. Lett.* **92**, 222502 (2008).
- [10] M. T. Björk, A. Fuhrer, A. E. Hansen, M. W. Larsson, L. E. Fröberg, and L. Samuelson, Tunable effective  $g$ -factor in InAs nanowire quantum dots, *Phys. Rev. B* **72**, 201307 (2005).
- [11] Y. A. Nefyodov, A. V. Shchepetilnikov, I. V. Kukushkin, W. Dietsche, and S. Schmult,  $g$ -factor anisotropy in a GaAs/Al<sub>x</sub>Ga<sub>1-x</sub>As quantum well probed by electron spin resonance, *Phys. Rev. B* **83**, 041307 (2011).
- [12] G. Sallen, B. Urbaszek, M. M. Glazov, E. L. Ivchenko, T. Kuroda, T. Mano, S. Kunz, M. Abbarchi, K. Sakoda, D. Lagarde, A. Balocchi, X. Marie, and T. Amand, Dark-Bright Mixing of Interband Transitions in Symmetric Semiconductor Quantum Dots, *Phys. Rev. Lett.* **107**, 166604 (2011).

- [13] T. P. M. Alegre, F. G. G. Hernández, A. L. C. Pereira, and G. Medeiros-Ribeiro, Landé  $g$  Tensor in Semiconductor Nanostructures, *Phys. Rev. Lett.* **97**, 236402 (2006).
- [14] A. Schwan, B. Meiners, A. Greilich, D. R. Yakovlev, M. Bayer, A. D. B. Maia, A. A. Quivy, and A. B. Henriques, Anisotropy of electron and hole  $g$ -factors in (In, Ga)As quantum dots, *Appl. Phys. Lett.* **99**, 221914 (2011).
- [15] S. Wu *et al.*, Anisotropies of the  $g$ -factor tensor and diamagnetic coefficient in crystal-phase quantum dots in InP nanowires, *Nano Res.* **12**, 2842 (2019).
- [16] V. V. Belykh, D. R. Yakovlev, J. J. Schindler, E. A. Zhukov, M. A. Semina, M. Yacob, J. P. Reithmaier, M. Benyoucef, and M. Bayer, Large anisotropy of electron and hole  $g$ -factors in infrared-emitting InAs/InAlGaAs self-assembled quantum dots, *Phys. Rev. B* **93**, 125302 (2016).
- [17] V. Jovanov, T. Eissfeller, S. Kapfinger, E. C. Clark, F. Klotz, M. Bichler, J. G. Keizer, P. M. Koenraad, G. Abstreiter, and J. J. Finley, Observation and explanation of strong electrically tunable exciton  $g$ -factors in composition engineered In(Ga)As quantum dots, *Phys. Rev. B* **83**, 161303 (2011).
- [18] T. Nakaoka, T. Saito, J. Tatebayashi, and Y. Arakawa, Size, shape, and strain dependence of the  $g$ -factor in self-assembled In(Ga)As quantum dots, *Phys. Rev. B* **70**, 235337 (2004).
- [19] H. M. G. A. Tholen, J. S. Wildmann, A. Rastelli, R. Trotta, C. E. Pryor, E. Zallo, O. G. Schmidt, P. M. Koenraad, and A. Y. Silov, Strain-induced  $g$ -factor tuning in single InGaAs/GaAs quantum dots, *Phys. Rev. B* **94**, 245301 (2016).
- [20] H. M. G. A. Tholen, J. S. Wildmann, A. Rastelli, R. Trotta, C. E. Pryor, E. Zallo, O. G. Schmidt, P. M. Koenraad, and A. Y. Silov, Active tuning of the  $g$ -tensor in InGaAs/GaAs quantum dots via strain, *Phys. Rev. B* **99**, 195305 (2019).
- [21] T. M. Godden, J. H. Quilter, A. J. Ramsay, Y. Wu, P. Brereton, I. J. Luxmoore, J. Puebla, A. M. Fox, and M. S. Skolnick, Fast preparation of a single-hole spin in an InAs/GaAs quantum dot in a Voigt-geometry magnetic field, *Phys. Rev. B* **85**, 155310 (2012).
- [22] F. Klotz, V. Jovanov, J. Kierig, E. C. Clark, D. Rudolph, D. Heiss, M. Bichler, G. Abstreiter, M. S. Brandt, and J. J. Finley, Observation of an electrically tunable exciton  $g$ -factor in InGaAs/GaAs quantum dots, *Appl. Phys. Lett.* **96**, 053113 (2010).
- [23] T. Nakaoka, T. Saito, J. Tatebayashi, S. Hirose, T. Usuki, N. Yokoyama, and Y. Arakawa, Tuning of  $g$ -factor in self-assembled In(Ga)As quantum dots through strain engineering, *Phys. Rev. B* **71**, 205301 (2005).
- [24] W. Sheng,  $g$ -factor tuning in self-assembled quantum dots, *Appl. Phys. Lett.* **96**, 133102 (2010).
- [25] B. J. Witek, R. W. Heeres, U. Perinetti, E. P. A. M. Bakkers, L. P. Kouwenhoven, and V. Zwiller, Measurement of the  $g$ -factor tensor in a quantum dot and disentanglement of exciton spins, *Phys. Rev. B* **84**, 195305 (2011).
- [26] D. N. Krizhanovskii, A. Ebbens, A. I. Tartakovskii, F. Pulizzi, T. Wright, M. S. Skolnick, and M. Hopkinson, Individual neutral and charged  $\text{In}_x\text{Ga}_{1-x}\text{As-GaAs}$  quantum dots with strong in-plane optical anisotropy, *Phys. Rev. B* **72**, 161312 (2005).
- [27] A. Zrenner, E. Beham, S. Stufler, F. Findeis, M. Bichler, and G. Abstreiter, Coherent properties of a two-level system based on a quantum-dot photodiode, *Nature* **418**, 612 (2002).
- [28] A. J. Ramsay, S. J. Boyle, R. S. Kolodka, J. B. B. Oliveira, J. Skiba-Szymanska, H. Y. Liu, M. Hopkinson, A. M. Fox, and M. S. Skolnick, Fast Optical Preparation, Control, and Readout of a Single Quantum Dot Spin, *Phys. Rev. Lett.* **100**, 197401 (2008).
- [29] J. D. Mar, J. J. Baumberg, X. Xu, A. C. Irvine, and D. A. Williams, Ultrafast high-fidelity initialization of a quantum-dot spin qubit without magnetic fields, *Phys. Rev. B* **90**, 241303 (2014).
- [30] A. J. Ramsay, A review of the coherent optical control of the exciton and spin states of semiconductor quantum dots, *Semicond. Sci. Tech.* **25**, 103001 (2010).
- [31] T. Nakaoka, S. Tarucha, and Y. Arakawa, Electrical tuning of the  $g$ -factor of single self-assembled quantum dots, *Phys. Rev. B* **76**, 041301 (2007).
- [32] J. H. Quilter, A. J. Brash, F. Liu, M. Glässl, A. M. Barth, V. M. Axt, A. J. Ramsay, M. S. Skolnick, and A. M. Fox, Phonon-Assisted Population Inversion of a Single InGaAs/GaAs Quantum Dot by Pulsed Laser Excitation, *Phys. Rev. Lett.* **114**, 137401 (2015).
- [33] Y. Wu, I. M. Piper, M. Ediger, P. Brereton, E. R. Schmidgall, P. R. Eastham, M. Hugues, M. Hopkinson, and R. T. Phillips, Population Inversion in a Single InGaAs Quantum Dot Using the Method of Adiabatic Rapid Passage, *Phys. Rev. Lett.* **106**, 067401 (2011).
- [34] A. Widhalm, A. Mukherjee, S. Krehs, N. Sharma, P. Kölling, A. Thiede, D. Reuter, J. Förstner, and A. Zrenner, Ultrafast electric phase control of a single exciton qubit, *Appl. Phys. Lett.* **112**, 111105 (2018).
- [35] S. Stufler, P. Ester, A. Zrenner, and M. Bichler, Ramsey Fringes in an Electric-Field-Tunable Quantum Dot System, *Phys. Rev. Lett.* **96**, 037402 (2006).
- [36] S. J. Boyle, A. J. Ramsay, A. M. Fox, M. S. Skolnick, A. P. Heberle, and M. Hopkinson, Beating of Exciton-Dressed States in a Single Semiconductor InGaAs/GaAs Quantum Dot, *Phys. Rev. Lett.* **102**, 207401 (2009).
- [37] A. N. Vamivakas, Y. Zhao, C.-Y. Lu, and M. Atatüre, Spin-resolved quantum-dot resonance fluorescence, *Nature Phys.* **5**, 198 (2009).
- [38] Y.-M. He, Y. He, Y.-J. Wei, D. Wu, M. Atatüre, C. Schneider, S. Höfling, M. Kamp, C.-Y. Lu, and J.-W. Pan, On-demand semiconductor single-photon source with near-unity indistinguishability, *Nature Nanotech.* **8**, 213 (2013).
- [39] A. J. Shields, M. P. O'Sullivan, I. Farrer, D. A. Ritchie, K. Cooper, C. L. Foden, and M. Pepper, Optically induced bistability in the mobility of a two-dimensional electron gas coupled to a layer of quantum dots, *Appl. Phys. Lett.* **74**, 735 (1999).
- [40] J. Wunderlich, B. Kaestner, J. Sinova, and T. Jungwirth, Experimental Observation of the Spin-Hall Effect in a Two-Dimensional Spin-Orbit Coupled Semiconductor System, *Phys. Rev. Lett.* **94**, 047204 (2005).
- [41] D. Najer, I. Söllner, P. Sekatski, V. Dolique, M. C. Löbl, D. Riedel, R. Schott, S. Starosielec, S. R. Valentin, A.

- D. Wieck, N. Sangouard, A. Ludwig, and R. J. Warburton, A gated quantum dot strongly coupled to an optical microcavity, *Nature* **575**, 622 (2019).
- [42] C. Santori, D. Fattal, J. Vučković, G. S. Solomon, and Y. Yamamoto, Indistinguishable photons from a single-photon device, *Nature* **419**, 594 (2002).
- [43] J. D. Mar, X. L. Xu, J. J. Baumberg, F. S. F. Brossard, A. C. Irvine, C. Stanley, and D. A. Williams, Bias-controlled single-electron charging of a self-assembled quantum dot in a two-dimensional-electron-gas-based  $n - i$ -Schottky diode, *Phys. Rev. B* **83**, 075306 (2011).
- [44] K. Peng, S. Wu, X. Xie, J. Yang, C. Qian, F. Song, S. Sun, J. Dang, Y. Yu, S. Xiao, and X. Xu, Tuning the carrier tunneling in a single quantum dot with a magnetic field in Faraday geometry, *Appl. Phys. Lett.* **114**, 091109 (2019).
- [45] J. D. Mar, X. L. Xu, J. J. Baumberg, A. C. Irvine, C. Stanley, and D. A. Williams, Voltage-controlled electron tunneling from a single self-assembled quantum dot embedded in a two-dimensional-electron-gas-based photovoltaic cell, *J. Appl. Phys.* **110**, 053110 (2011).
- [46] K. Peng, S. Wu, X. Xie, J. Yang, C. Qian, F. Song, S. Sun, J. Dang, Y. Yu, S. Shi, J. He, and X. Xu, Giant Photocurrent Enhancement by Coulomb Interaction in a Single Quantum Dot for Energy Harvesting, *Phys. Rev. Appl.* **11**, 024015 (2019).
- [47] J. D. Mar, J. J. Baumberg, X. L. Xu, A. C. Irvine, and D. A. Williams, Precise measurements of the dipole moment and polarizability of the neutral exciton and positive trion in a single quantum dot, *Phys. Rev. B* **95**, 201304 (2017).
- [48] H. W. van Kesteren, E. C. Cosman, W. A. J. A. van der Poel, and C. T. Foxon, Fine structure of excitons in type-II GaAs/AlAs quantum wells, *Phys. Rev. B* **41**, 5283 (1990).
- [49] M. Bayer, G. Ortner, O. Stern, A. Kuther, A. A. Gorbunov, A. Forchel, P. Hawrylak, S. Fafard, K. Hinzer, T. L. Reinecke, S. N. Walck, J. P. Reithmaier, F. Klopf, and F. Schäfer, Fine structure of neutral and charged excitons in self-assembled In(Ga)As/(Al)GaAs quantum dots, *Phys. Rev. B* **65**, 195315 (2002).
- [50] K. Peng, S. Wu, J. Tang, F. Song, C. Qian, S. Sun, S. Xiao, M. Wang, H. Ali, D. A. Williams, and X. Xu, Probing the Dark-Exciton States of a Single Quantum Dot Using Photocurrent Spectroscopy in a Magnetic Field, *Phys. Rev. Appl.* **8**, 064018 (2017).
- [51] K. G. Lagoudakis, K. A. Fischer, T. Sarmiento, K. Mueller, and J. Vučć, Hole-spin pumping and repumping in a  $p$ -type  $\delta$ -doped InAs quantum dot, *Phys. Rev. B* **90**, 121402 (2014).
- [52] V. V. Belykh, A. Greilich, D. R. Yakovlev, M. Yacob, J. P. Reithmaier, M. Benyoucef, and M. Bayer, Electron and hole  $g$ -factors in InAs/InAlGaAs self-assembled quantum dots emitting at telecom wavelengths, *Phys. Rev. B* **92**, 165307 (2015).
- [53] J. van Bree, A. Y. Silov, M. L. van Maasakkers, C. E. Pryor, M. E. Flatté, and P. M. Koenraad, Anisotropy of electron and hole  $g$  tensors of quantum dots: An intuitive picture based on spin-correlated orbital currents, *Phys. Rev. B* **93**, 035311 (2016).
- [54] W. Sheng and A. Babinski, Zero  $g$ -factors and nonzero orbital momenta in self-assembled quantum dots, *Phys. Rev. B* **75**, 033316 (2007).
- [55] W. Sheng, Landé  $g$ -factors in elongated InAs/GaAs self-assembled quantum dots, *Physica E* **40**, 1473 (2008).
- [56] J. Houel, J. H. Prechtel, A. V. Kuhlmann, D. Brunner, C. E. Kuklewicz, B. D. Gerardot, N. G. Stoltz, P. M. Petroff, and R. J. Warburton, High Resolution Coherent Population Trapping on a Single Hole Spin in a Semiconductor Quantum Dot, *Phys. Rev. Lett.* **112**, 107401 (2014).
- [57] J. H. Prechtel, A. V. Kuhlmann, J. Houel, A. Ludwig, S. R. Valentin, A. D. Wieck, and R. J. Warburton, Decoupling a hole spin qubit from the nuclear-spins, *Nat. Mater.* **15**, 981 (2016).
- [58] W. Sheng, S. J. Xu, and P. Hawrylak, Electron  $g$ -factor distribution in self-assembled quantum dots, *Phys. Rev. B* **77**, 241307 (2008).